Comparison of different spatial temperature data sources and resolutions for use in understanding intra-urban heat variation

Ayda Kianmehr [a,*], Theodore C. Lim [a], Xiaojiang Li [b]

[a] *School of Public and International Affairs, Virginia Polytechnic Institute and State University, Blacksburg, VA 24061, USA*
[b] *Department of Geography and Urban Studies, Temple University, Philadelphia, PA 19122, USA*

ARTICLE INFO

ABSTRACT

In this study, we investigate the compatibility of specific vulnerability indicators and heat exposure data and the suitability of spatial temperature-related data at a range of resolutions, to represent spatial temperature variations within cities using data from Atlanta, Georgia. For this purpose, we include various types of known and theoretically based vulnerability indicators such as specific street-level landscape features and urban form metrics, population-based and zone-based variables as predictors, and different measures of temperature, including air temperature (as vector-based data), land surface temperature (at resolution ranges from 30 m to 305 m), and mean radiant temperature (at resolution ranges from 1 m to 39 m) as dependent variables. Using regression analysis, we examine how different sets of predictors and spatial resolutions can explain spatial heat variation. Our findings suggest that the lower resolution of land surface temperature data, up to 152 m, and mean radiant temperature data, up to 15 m, may still satisfactorily represent spatial urban temperature variation caused by landscape elements. The results of this study have important implications for heat-related policies and planning by providing insights into the appropriate sets of data and relevant resolution of temperature measurements for representing spatial urban heat variations.

1. Introduction

Cities worldwide are growing fast to accommodate the increasing global population. According to the United Nations New Urban Agenda, by 2050, the world's population is expected to double, which makes urbanization an inevitable trend (Habitat, 2017). The excess heat resulting from deforestation, land cover change, and the prevalence of impervious surfaces is great enough to raise the cities' average temperature by several degrees over the non-urbanized and rural parts and lead to a known phenomenon called the urban heat island effect (Oke, 1987). Increased temperature in cities impacts human health and well-being in several ways. However, the associated effects of heat exposure in cities are not spatially uniform (Chen et al., 2022). Land use, landscape features, surface covers, and morphological parameters make temperature distribution in cities disproportionate and cause disparities in the burden of heat exposure across sociodemographic groups (Hsu et al., 2021; Voelkel et al., 2018). While proactive heat mitigation strategies at the local level are integral to compensate for the severity of extreme heat exposure, a lack of spatially explicit information on hotspots would undermine the specificity and applicability of the policies

(Preston et al., 2011). Hence, the demand for systematic representations of spatial heat heterogeneity within cities is rising (Meng et al., 2018; Peng et al., 2020).

Representation of heat exposure variation can be facilitated through empirical measurements, allowing the direct observation of spatial and temporal variation in temperatures. For example, LANDSAT and MODIS images are widely applied to classify land cover/ land use changes and assess the association between spatiotemporal factors and the urban heat island effect (Chen, 2021; Deilami et al., 2016; Guha et al., 2018; Mukherjee & Singh, 2020; Schwarz et al., 2011). While empirical techniques such as satellite imagery and *in-situ* temperature measurements have moderate spatial and temporal resolutions, physically based modeling may provide higher resolution exposure representation by involving an array of physical and meteorological parameters at finer scales. Finer scales may be especially useful when engaging with residents because they enable more convincing causal relationships linked to the variation in temperatures (Berardi et al., 2020; Gunawardena & Steemers, 2019; Kianmehr & Lim, 2022). Moreover, modeling can incorporate more salient aspects of urban heat than remotely sensed infrared reflectance. For example, solar irradiance geometry models

apply urban 3D models and meteorological data to estimate citizens' thermal comfort level in urban areas with a high resolution and through a human-centric point of view. Ultimately, however, the value of finer scale data depends on its intended use. For example, Wu et al. (2019) found that coarse regional air temperature data were sufficient to predict heat mortality during heat waves.

Urban planners are increasingly concerned with how decisions about the built environment can influence microclimate, giving rise to a need for models that can more precisely relate elements in the built environment with temperature impact (Keith & Meerow, 2022). Identification of underlying reasons for heat vulnerability and exposure variations within cities requires choosing appropriate proxies and relevant resolution of data (Karanja & Kiage, 2021). In recent years, advancements in "big data" acquisition and analysis have facilitated the operationalization of the known and theoretically based predictors, which could theoretically result in more precise predictions and explanations of spatial heat vulnerability associated with landscape elements. For instance, Google Application Programming Interface (API) for street view images (Google Street View, hereafter, "GSV") provides easy access to the extensive and invaluable sets of data taken from human-centric views (Middel et al., 2019), which allows for capturing three-dimensional elements with much higher resolution (Xu et al., 2012). In urban heat studies, street-level landscape features and urban form metrics derived from profile-based GSV images have been applied to identify the type, density, and distribution of urban greenery (Li et al., 2015b), track the temporal change of green index (Li, 2021b), and assess the accessibility of different neighborhoods and communities to the green areas (Li et al., 2015a). This promising source of data, coupled with other social indicators of heat vulnerability, such as poverty rate, educational attainment, ethnicity, gender, age, and historical segregation practices (Cutter et al., 2003; Dialesandro et al., 2021; Hoffman et al., 2020; Uejio et al., 2011; Wilson, 2020) can be used to create a picture of physical and social vulnerability of different localities toward the heat risk with a high resolution.

Whereas such suites of individual indicators leverage fine-scale analysis of temperature variations, aggregation techniques can change the nature of the gained information (Abson et al., 2012). A mismatch in spatial resolution among exposure data and physical and social vulnerability indicators (hereafter, vulnerability indicators) obstructs the consistent development of metrics and accurate representation of disparities (Cutter & Finch, 2008; Ho et al., 2015). This issue mainly emanates from a phenomenon called Modifiable Areal Unit Problem (MAUP) (Openshaw, 1984). The MAUP happens as the result of two distinct yet related conditions: the scale problem and the zoning effect (Fotheringham & Wong, 1991). The scale problem is associated with the aggregation of areal units' (e.g., pixel) data into the adjacent units, resulting in coarser units of analysis with the same areal size. In contrast, the zoning problem is related to the use of an alternative unit of analysis with different sizes while the total number of units is held constant (Ho et al., 2015; Ju et al., 2021). Both circumstances can change the results in multivariate analyses (Jelinski & Wu, 1996). For example, when the unit of analysis for the exposure and vulnerability analysis is determined arbitrarily, the analysis results may not reflect the real spatial heat heterogeneity. Such biased results would also hinder the accurate identification of suitable exposure and vulnerability indicators and proxies.

Selecting appropriate vulnerability indicators and data resolutions congruent with system dynamics is challenging, yet it is central to ascertaining appropriate heat mitigation strategies. There are many conceptual models in heat-related studies that scrutinize heat vulnerability at a fine scale to benefit site-specific policy-making (Conlon et al., 2020; Johnson et al., 2012; Mushore et al., 2018; Song et al., 2020). However, except for a few studies (Ho et al., 2015; Sobrino et al., 2012; Zhou et al., 2014), the literature lacks systematic analysis of data types and resolutions needed for the accurate detection of spatial heat variation and explainability of that variation. Therefore, this paper aims to explore what information can be gained about physical and social aspects of heat vulnerability and heat exposure through a data-driven approach that fuses different kinds of spatial data at a range of resolutions. As high-resolution data is not readily available for many locations due to the resource limitations and computational expenses (Deilami et al., 2018), this study specifically aims to evaluate the feasibility of using lower-resolution temperature data and new sources of vulnerability indicators to explain intra-urban heat variations. The key research questions this study seeks to answer are: first, what is the satisfactory range of exposure data resolution for accurately representing spatial temperature variations? Second, which groups of vulnerability indicators can better explain the variations in air temperature, land surface temperature, and mean radiant temperature? And, finally, what is the effect magnitude of specific landscape features and urban form metrics on changing temperatures? And how do the direction and magnitude of this effect differ in the whole study area and high-density zones?

2. Data and method

2.1. Study area

Taking the city of Atlanta, Georgia, in the Southern United States as the case study, we systematically assess the compatibility of specific vulnerability indicators and temperature data and the suitability of specific spatial data at a range of resolutions for the representation of spatial temperature variations within cities. For this purpose, we employ various types of predictors, including specific street-level features, socio-demographic-based, and zone-based variables, to explain spatial air temperature (AT), land surface temperature (LST), and mean radiant temperature (MRT) variation within the city of Atlanta. The vector and raster-based data, including field measurements of air temperature, satellite imagery, and modeling data of various resolutions, are treated as dependent variables in the multivariate regression analyses.

The city of Atlanta has a population of around 500,000 and is also growing quickly (United States Census Bureau, 2021). Located in Fulton County, the city of Atlanta is characterized by humid subtropical weather with four seasons (Sun et al., 2018). Simulation results predict that Atlanta will experience higher frequency and longer duration of heatwaves (Habeeb et al., 2015). According to a survey, only 57% of respondents can afford or use central air conditioning when needed (Larsen et al., 2022). In addition, there is a disproportionate exposure to the heat in Atlanta, where the greater burden of the urban heat island effect falls on the poor (Chakraborty et al., 2019).

2.2. Data

According to studies such as Adger (2006), Guillard-Gonçalves and Zêzere (2018) and Turner et al. (2003), in this paper, we refer to vulnerability indicators as the composite of biophysical and socioeconomic indices. Based on theories related to physical and social vulnerability, we used three types of vulnerability indicators, including street-level landscape features and urban form metrics, population-based, and zone-based data, as explanatory variables in the regression analyses. Moreover, to study spatial temperature variation, we employed three exposure data types as dependent variables in multivariate regression analyses: air temperature, land surface temperature, and mean radiant temperature. Thermal comfort provided by shading and wind speed is highly dependent on fine-scale landscape features and urban form metrics. Studying the variations in thermal comfort and shading was the primary motivation for using the mean radiant temperature as one of the exposure data types in this study. Air and surface temperature might not capture thermal comfort as thoroughly as other heat indexes, yet they are the most prevalent and accessible types of temperature data and are worth further exploration to test their suitability for representing spatial heat variations.

Table 1
Information about the original resolution and distribution of each type of heat exposure data.

	Air Temperature	Land Surface Temperature	Mean Radiant Temperature
Original resolution	23,386 points with a 10 m distance	At the resampled ~100 ft (30 m) resolution	~2 ft (1 m)
Minimum	25.45 C	31.55 C	34.71 C
Maximum	30.48 C	50.84 C	58.14 C
Mean	27.95 C	40.11 C	49.08 C
Standard deviation	0.81	4.13	7.46

2.2.1. Exposure data

2.2.1.1. Air Temperature (AT). Air temperature data were obtained from urban heat campaign (UHC) measurements for Atlanta. Funded by NOAA, over the past five years, the urban heat campaign has taken place in several localities in the U.S. (Mapping Campaigns, 2022). In this study, we used the afternoon measurements data (3:00 pm–4:00 pm) of the urban heat campaign in Atlanta, which took place on September 4th, 2021, and contained 23,386 observation points. Morning and evening measurements from this campaign are also available. However, given the significance of heat-related studies during the hottest hours of the day and one of the purposes of this study, which is to analyze the shading effect of street-level elements, we utilized the afternoon data from the UHC measurements. Further information about air temperature data employed in this study can be found in Table 1. This vector-based source of data is treated as one of the dependent variables in our multivariate regression analyses. In Fig. 1, we represent the normalized (scaled to the maximum-minimum range) spatial distribution of air temperature along with other types of heat exposure data used in this study (land surface temperature and mean radiant temperature) for comparison purposes. Fig. 1(a) shows the normalized spatial distribution of air temperature data, the study area, and the observation points of this study.

2.2.1.2. Land Surface Temperature (LST). The land surface temperature data was acquired through the bulk download of Landsat 8 images from the United States Geological Survey (USGS) website. Thermal infrared sensor (TIRS) images of Atlanta for the summer months (June 1 – September 30) of years between 2019 and 2021 were collected (a total of 14 scenes) and used for processing the raster data, including masking clouds and handling missing pixels. In the next step, the actual daytime land surface temperature for each grid point was calculated by converting the raster values into degrees of centigrade and taking means across all scenes. As a result, a single-layer daytime land surface temperature image was created for Atlanta city. We shall note here the original resolution of the Landsat TIR sensor is 100 m. However, the resolution of raster data used in this study has been changed to 30 m as a part of the Analysis Ready Data (ARD) dataset, prepared by the USGS, to match the resolution of other (visible band) data distributed in ARD. For more information about the resolution of Landsat images please refer to the USGS website (USGS, 2023). This dataset was also used as a dependent variable in multivariate regression analysis (Fig. 1(b)).

2.2.1.3. Mean Radiant Temperature (MRT). MRT more closely represents the thermal comfort that humans feel because it is derived by summing all shortwave and longwave radiation fluxes that the human body is exposed to (both directly and reflected) (Lindberg et al., 2008). However, this means that MRT cannot easily be measured as a spatial dataset and is usually calculated through mathematical modeling. Using SOLWEIG (SOlar and LongWave Environmental Irradiance Geometry) model, besides spatial variations of 3D radiation fluxes, we simulated the shadow pattern and the sky view factor of Atlanta's urban settings, taking into account the influence of shade on the thermal comfort of the

human body. The two major inputs of the model are terrain features including ground topography and building configurations, and meteorological data, such as air temperature, relative humidity, wind speed, direct radiation, and diffuse radiation (Li, 2021a). For Atlanta, meteorological data and the high-resolution (1 m) 3D urban model generated from LiDAR and aerial images were used as inputs of SOLWEIG to calculate the spatial distribution of average mean radiant temperature and, thus, the human outdoor thermal exposure level across neighborhoods. More information about the modeling process can be found in our previous study (Li, 2021a). This raster-based data also was treated as the dependent variable in our regression analysis (Fig. 1(c)). Further details about the distribution and original resolution of this dataset can be found in Table 1. LST and MRT data of Atlanta show a similar pattern for the distribution of hotspots in this city, where the highest land surface and mean radiant temperature were observed in industrial, high-density commercial, and office institutional zones. The most elevated air temperatures were observed in the southern part of the city, where the high-density residential and single-family residentials are located. The distinction between the distribution of hot spots and cool spots of air temperature and other measures of heat, such as land surface temperature, has been noted in other studies. This can be attributed to the anthropogenic activities and physical and landscape parameters that affect air temperature variations in urban areas (Amani-Beni et al., 2022).

2.2.2. Heat vulnerability indicators

2.2.2.1. Landscape features and urban form metrics. In this study, vulnerability indicators refer to both biophysical and social aspects of vulnerability, such as lack of vegetation and shading, increased sky view factor, the prevalence of impervious surfaces, and a larger population of marginalized groups. In our study, landscape features and urban form metrics are considered as one of the subsets of vulnerability indicators and refer to morphological characteristics such as sky view factor and street-level built environment and landscape features that pedestrians can directly perceive. To collect data related to such physical aspects of heat vulnerability, we used Google Street View images of Atlanta. Using the Urban Heat Campaign measurement point locations, we obtained a list of available images in different years and months for those measurement points. We filtered the image list for the September years between 2017 and 2019 to get the list of the most recent and relevant images for download. This list contained 12,321 panorama identification numbers (I.D.). As for each panorama I.D., four images are available; overall, we downloaded 49,284 images for those specific locations.

To quantify the landscape features and built environment of downloaded images, we used Pyramid Scene Parsing Network (PSPNet), a superior framework for pixel-level predictions (Zhao et al., 2017). This image scene parsing and semantic segmentation algorithm enabled us to quantify 150 features (including buildings, trees, grass, road, sky, water, person, and car) that appeared in the downloaded images and analyze the physical characteristics of desired locations. Fig. 2, created by the authors, illustrates the process of quantifying street-level elements in Google Street View images using PSPNet.

We further used GSV panoramas to calculate the sky view factor (SVF), which refers to the ratio between the radiance received by a planar ground and the entire hemispheric radiation. The value of SVF ranges from 0 to 1, where 0 represents the total enclosure of the urban environment by trees or buildings, and one exhibits complete openness. We generated hemispherical images from the GSV panorama images using a geometrical transform model and quantified the visible portions of the sky to calculate the SVF of each observation point. For further details about calculating SVF from GSV images, refer to Li and Ratti (2018).

2.2.2.2. Population-based data. Besides physical and morphological
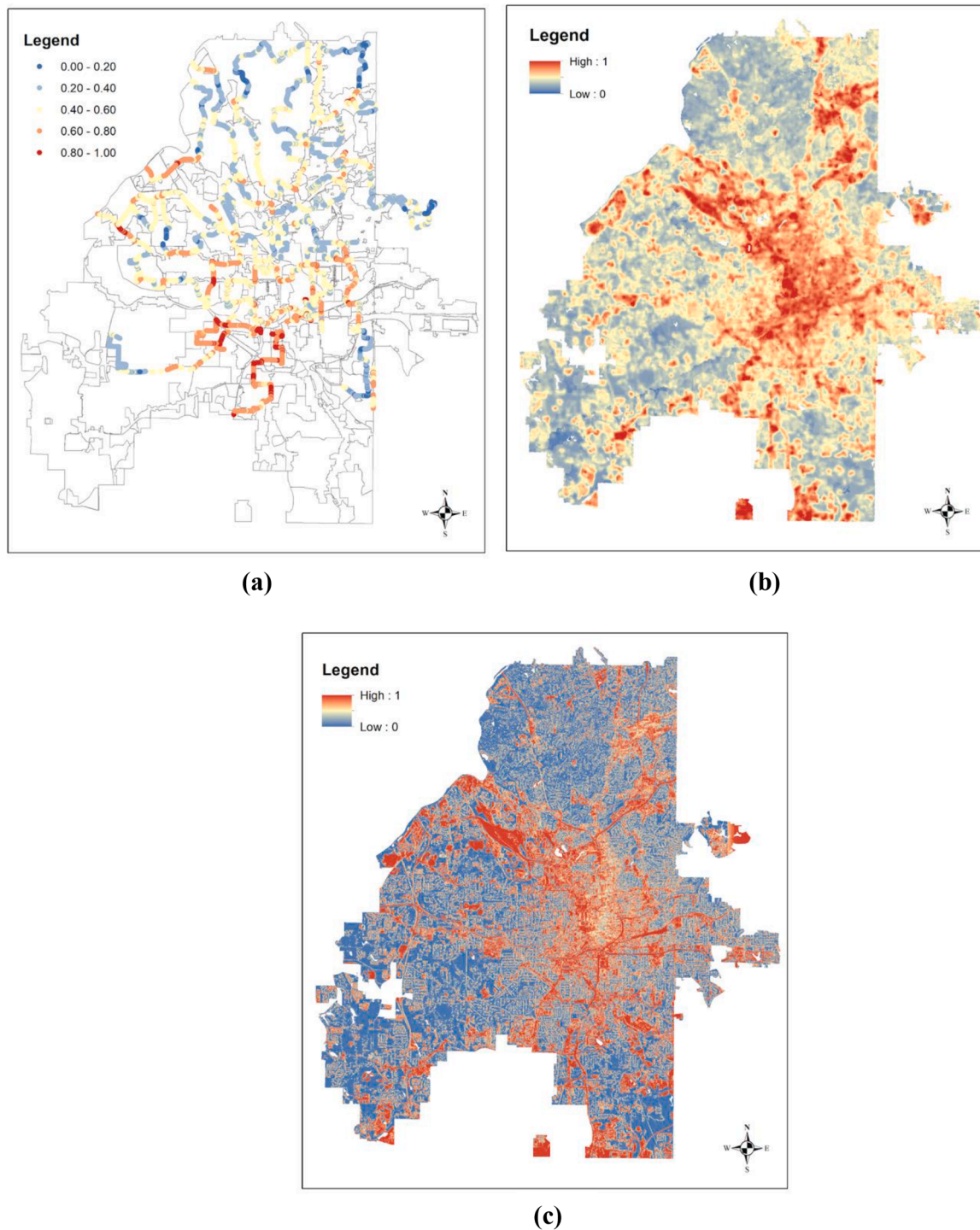
(a)

(b)

(c)

Fig. 1. Normalized spatial distribution of air temperature (a), land surface temperature (b), and mean radiant temperature (c), the three dependent variables used in the regression analyses.

metrics, sociodemographic variables have been shown to have explanatory power over spatial temperature distribution (Karanja & Kiage, 2021). This is because of discriminatory housing and urban planning processes and residential segregation. Socioeconomic indices such as race, income, education, gender, and age can be used to assess the social aspects of heat vulnerability and risk associated with heat in different localities (Harlan et al., 2006; Uejio et al., 2011; Wilson, 2020). We obtained population data for our temperature observation points from the City of Atlanta's open data portal, including total population, population density, and the percentage of each race (White, African

American, Hispanic, and Asian) in 2010. We included those variables in stepwise regression analysis to identify the most important population-based variables to include in our regression models.

2.2.2.3. Zone-based data. Urban heat island intensity is associated with the dominant land use and land cover zones (Weng et al., 2007; Yang et al., 2017). The urban thermal environment in a city varies due to the differences in land use and surface characteristics (Chen et al., 2023; Hart & Sailor, 2009), and the effects of these differences may not be captured through the street-centric landscape elements derived from

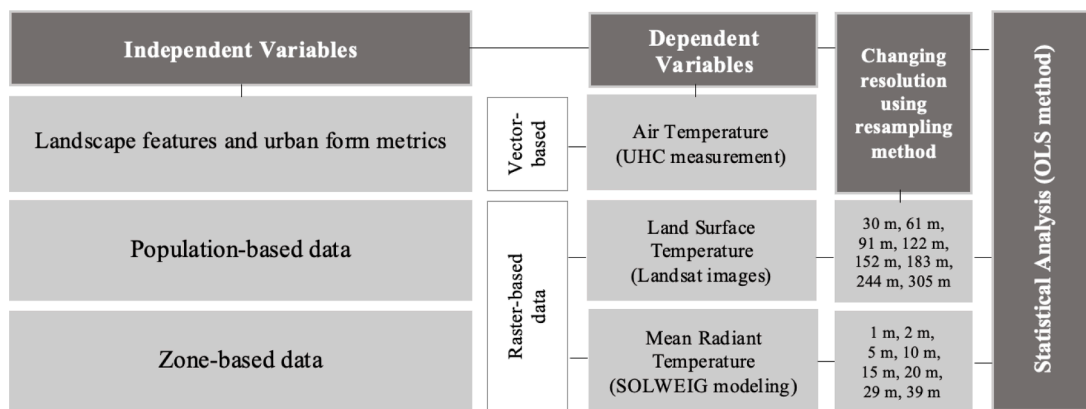**Fig. 2.** Street View image from Google API (left) and the result of image parsing using PSPNet (right).

Fig. 3. Workflow diagram of the present study.

Table 2
Selected independent and dependent variables for multivariate regression analyses.

Independent Variables	Dependent Variables
Xg: Landscape features and urban form metrics (GSV- driven variables): Plant, grass, sidewalk, path, house, building, car, water, sky view factor (SVF)	AT, LST, and MRT (Various resolutions)
Xp: Population-based variables: Population, black population	
Xz: Zone-based variables: Zone class categories	

GSV. To incorporate the effect of broader land use and land cover characteristics in the analysis of intra-urban heat variation, we included Atlanta's zone class categories in our analyses. Atlanta's zone class categories were obtained from the open data portal of the City of Atlanta. We also examined other categorical types of data, such as land use, neighborhood planning units, and statistical areas. However, we found that the zone class categories contributed the most to changes in temperatures.

2.3. Methodology

As discussed above, a variety of methods were adopted to extract and prepare data for statistical analysis. Fig. 3 reviews the workflow of the present study.

2.3.1. Changing data resolution

To examine the suitability of specific spatial data at a range of resolutions for the representation of spatial temperature variations, we downgraded the resolution of raster-based exposure data (LST and MRT)

using the resampling method (Bilinear interpolation technique) in GIS software. The bilinear interpolation technique, through calculating the weighted average of each of four nearby grid cells, allowed us to generate new values for the output grid cells and downgrade the resolution of raster data. For the LST data, we downgraded the resampled resolution of ~100 ft (30 m) to 200 ft (~61 m), 300 ft (~91 m), 400 ft (~122 m), 500 ft (~152 m), 600 ft (~183 m), 800 ft (~ 244 m), and 1000 ft (~305 m). Also, for the MRT, we reduced the original resolution from ~2 ft (1 m) to 8 ft (~2 m), 16 ft (~5 m), 32 ft (~10 m), 48 ft (~15 m), 64 ft (~20 m), 96 ft (~29 m), and 128 ft (~39 m). We should note here that as our air temperature data is vector-based, changing resolution does not apply to this data type in our analysis. So, we treated LST and MRT with various spatial resolutions alongside the original resolution of AT as dependent variables in our multivariate regression analyses.

We used coefficient determination (R-squared) that measures the goodness-of-fit to compare the explanatory power of land surface and mean radiant temperature data at a range of resolutions for the representation of spatial heat variations.

2.3.2. Statistical analyses

To identify the important variables to include in our regression models, we used forward and backward stepwise regression. Based on the outputs of this feature selection method, we developed various models with different groups of predictors (i.e., landscape features and urban form metrics, population-based, zone-based variables) and dependent variables (i.e., AT, LST, and MRT of various resolutions). We also checked for multicollinearity and removed variables that showed a strong relationship with each other. The final set of selected variables for the regression model can be found in Table 2. We used JMP software to
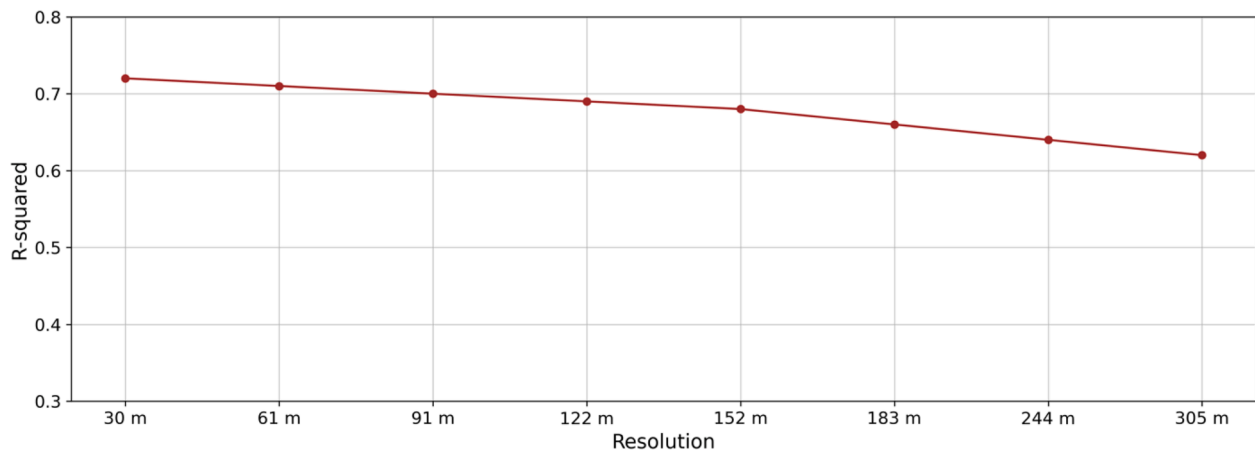
Fig. 4. Regression results (R-squared value) of LST models with different resolutions.
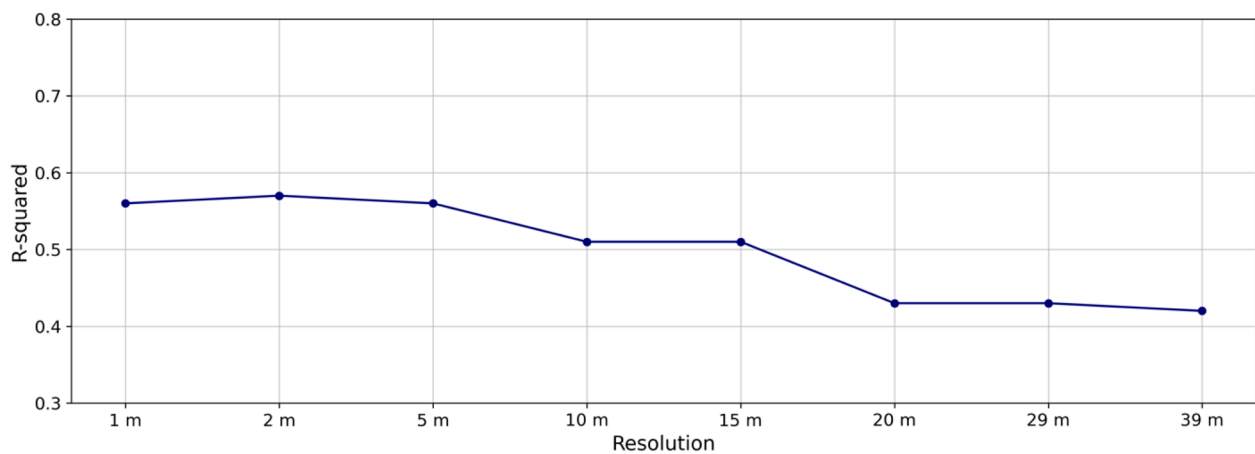

Fig. 5. Regression results (R-squared value) of MRT models with different resolutions.

perform ordinary least squares (OLS) regression and used resulting R-squared (and adjusted R-squared for the nested models) values to study the power of different groups of predictors in explaining the variations in AT, LST, and MRT over a range of resolutions (Eq. (1)). The initial total observation points in our study were 8895, and each observation point was located at least a 10-meter distance from the adjacent points. Eq. (1) shows the statistical specification of the ordinary least squares regression.

$$Y_i = \beta_1 X_{g,i} + \beta_2 X_{p,i} + \beta_3 X_{z,i} + \varepsilon_i \qquad (1)$$

where, Y_i is one of the dependent variables, including AT, LST, and MRT at a specific resolution at location i; $X_{g,i}$ is the vector of landscape features, and urban form metrics (GSV-driven variables) observed at location i; $X_{p,i}$ is the vector of population-based variables in the area in which location i falls; $X_{z,i}$ is the vector of zone-based variables in which location i falls; β_1, β_2, and β_3 are vectors of the estimated coefficients of predictor variables; ε_i is the error term observed for location i.

Following OLS estimation of the coefficients, we also checked for spatial autocorrelation. Details about those analyses can be found in Appendix A.

To further explore the role of shading and vegetation in temperature variations, we investigated the direction and magnitude of the effect of specific landscape features and urban form metrics (such as plants, buildings, and the sky view factor) on temperature exposure data using the standardized regression coefficient (SRC). The SRC ranges between −1 and +1 and indicates both the direction and magnitude of changes in the response variable that occur with changes in the independent

variable. We also estimated regressions using two subsets of the data: (1) the whole study area and (2) high-density zones (high-density residential, commercial, and office institutional zones) only. The reason for comparing the estimated coefficients on the high-density subset of the data is that we hypothesized very tall buildings, by providing shading and reducing the sky view factor in these areas, would lower the mean radiant temperature (MRT) and perhaps moderate the effect of vegetation.

3. Results

3.1. Spatial resolution effect

Figs. 4 and 5 show the R-squared value of the regression model (Eq. (1)) of LST and MRT data at a range of resolutions. The Y axis in these plots represents the R-squared values of the regression models, and the X axis shows the resolution of dependent variables (LST and MRT). According to Fig. 4, the R-squared value of the regression model or the explanatory power of the independent variables included in the model did not change significantly when the LST data resolution was downgraded to 500 ft (~152 m). By lowering the resolution after 500 ft, the R-squared value started to drop at a higher rate. Overall, downgrading the LST data resolution from ~100 ft (30 m) to 1000 ft (~305 m) changed the R-squared value from the range of 0.7 to 0.6. This pattern suggests that even lower resolutions of LST data can still be appropriate for explaining the variations in land surface temperature. A similar pattern is observed for MRT while decreasing spatial resolution (Fig. 5).
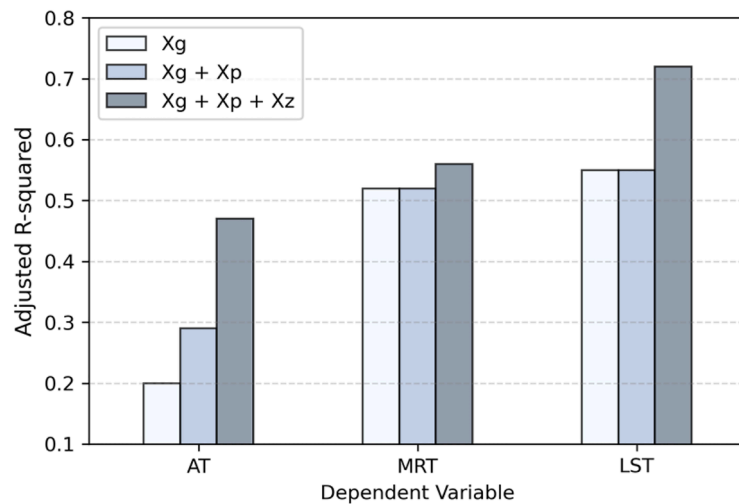
Fig. 6. Comparing regression models with different groups of predictors and dependent variables (with original resolutions).
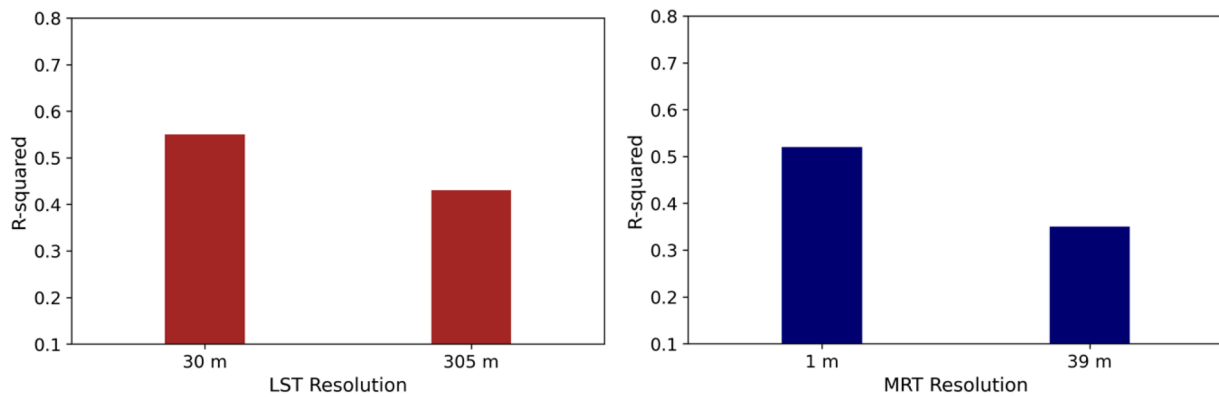

Fig. 7. Comparing the explanatory power of GSV-driven variables regression models with different resolutions of LST (left) and MRT (right) data.

Table 3
Standardized regression coefficients with only GSV-driven variables included in the model.

	LST Original resolution (30 m)	305 m resolution	MRT Original resolution (1 m)	39 m Resolution
Plant******	−0.09*	−0.08*	−0.08*	−0.09*
Grass	−0.20*	−0.21*	−0.09*	−0.10*
Sidewalk	0.05*	0.03*	−0.00	0.05*
Path	−0.02*	−0.01	−0.01	−0.01
House	−0.02*	−0.03*	−0.04*	−0.06*
Building	0.33*	0.29*	0.05*	0.06*
Car	0.07*	0.08	−0.00	0.02*
Water	−0.00	−0.01	0.01	0.02*
SVF	0.42*	0.34*	0.62*	0.47*

* Significant at 95% confidence level.
** Plant in this table refers to any types of greenery, including small trees, shrubs, herbs, and mosses which are distinct from grass.

The higher range of R-squared values of the regression models with LST data at various resolutions implies groups of independent variables considered in this study (Table 2) have higher explanatory power for explaining variations in land surface temperature compared to the mean radiant temperature.

3.2. The explanatory power of different groups of vulnerability indicators

As mentioned in the previous sections, we included landscape features and urban form metrics (GSV-driven variables), population-based, and zone-based variables in our regression model as predictors. To study the effect of each group of these variables separately, we included them in the model one by one, ran the regression model one at a time, and compared the adjusted R-squared. As different numbers of variables were included in each model, an F-test also was performed to identify whether the more complex models (models with more variables) have a significant improvement over the simpler models (models with a reduced number of variables). Pairwise comparisons of the F-ratio (using the ANOVA test) demonstrate that more complex models offer significant improvements over the simpler models for each dependent variable. More details about the F-test comparisons can be found in Appendix B.

Fig. 6 shows the adjusted R-squared values of each of those regression models with air temperature, land surface temperature, and mean radiant temperature in their original resolutions (at the resampled ~100 ft (30 m) resolution for LST and ~2 ft (1 m) for MRT) as the dependent variables. According to this plot, the regression results for the LST data show the highest adjusted R-squared values (0.55, 0.55, 0.72) compared to the MRT (0.52, 0.52, 0.56) and AT (0.20, 0.29, 0.47). Moreover, this figure shows that the GSV-driven variables have higher explanatory power for explaining MRT and LST data variations than the air temperature. However, it appears that the population-based and especially the zone-based variables have the most important impacts in

Table 4
Standardized regression coefficients of specific landscape features and urban form metrics with all groups of variables included in the model.

	Whole Study Area			High-Density Residential, Commercial and Office Zone		
	AT	LST	MRT	AT	LST	MRT
		Original resolution (30 m)	Original resolution (1 m)		Original resolution (30 m)	Original resolution (1 m)
Plant	−0.11*	−0.04*	−0.05*	−0.06*	−0.04*	−0.08*
Grass	−0.18*	−0.07*	−0.02	−0.18*	−0.10*	−0.17*
Building	−0.02	0.21*	0.01	0.00	0.12*	−0.12*
SVF	0.11*	0.26*	0.55*	0.06*	0.09*	0.33*

* Significant at 95% confidence level.

Table A1
Moran's I test results.

	Moran's Index
AT	0.51
LST	0.59
MRT	0.24

Table A2
Comparison of the SLM, SEM, and OLS regression results (R-squared).

	SLM	SEM	OLS
AT model	0.78	0.79	0.28
LST model	0.87	0.88	0.56
MRT model	0.62	0.62	0.51

Table B1
Degrees of freedom, sum and mean squares of the response variables.

Model	Y	DF	Sum of Squares	Mean Square
Reduced 1 (Xg)	AT	8836	15,385.325	1.7412
Reduced 2 (Xg+Xp)	AT	8834	13,582.713	1.5375
Complete (Xg+Xp+Xz)	AT	8731	10,020.990	1.1477
Reduced 1 (Xg)	LST	8836	65,595.475	7.4237
Reduced 2 (Xg+Xp)	LST	8834	65,088.259	7.3679
Complete (Xg+Xp+Xz)	LST	8731	40,338.703	4.6202
Reduced 1 (Xg)	MRT	8836	231,002.781	26.1433
Reduced 2 (Xg+Xp)	MRT	8834	230,088.591	26.0458
Complete (Xg+Xp+Xz)	MRT	8731	209,149.756	23.9548

Table B2
F-test results for regression model relations.

	Partial F (Complete| Reduced 1)	Partial F (Complete| Reduced 2)	Partial F (Reduced 2| Reduced 1)
AT	29.5762*	30.1284*	586.1964*
LST	52.0632*	52.0083*	34.4201*
MRT	8.6882*	8.4864*	17.5496*

* Significant at 95% confidence level.

explaining the variations in air temperature. This fact suggests air temperature of different locations in a city is more associated with socio-demographic and land use/ land cover characteristics of the area rather than the landscape features and urban form characteristics.

In addition, the low adjusted R-squared value of the air temperature regression model with GSV-driven variables implies the air temperature data would not necessarily benefit from higher spatial resolution data collection since it is already not explainable by high-resolution landscape features and urban form metrics data. However, higher temporal resolution might mitigate the low explanatory power of these variables in regression models, which requires further investigation.

Based on Fig. 6, we also noticed while the population-based variables would help explain air temperature variations, they did not improve adjusted R-squared values for the MRT and LST regressions. However, the zone-based data had a positive effect in improving the adjusted R-squared value of the LST regression result. Overall, among variables considered in this study, landscape features and urban form metrics (GSV-driven variables) were found to be the most important groups of variables for explaining the variation in MRT and LST.

As the role of GSV-driven variables in explaining LST and MRT variations proved to be significant, we also studied the explanatory power of this group of variables with the lowest resolutions of LST and MRT data. Fig. 7 represents the results (R-squared) of regression models in which the GSV-driven variables were included as independent and the lowest resolution LST and MRT data as the dependent variables. We also reported the regression result with the original resolutions in this plot to compare the impact of data resolution on the explanatory power of this group of variables.

As expected, lowering data resolutions for LST and MRT lowered the explanatory power of the high-resolution GSV-driven variables. However, even in the lowest resolutions studied in this paper (1000 ft (~305 m) for the LST and 128 ft (~39 m) for the MRT data), those variables still showed a relatively moderate potential for explaining the variation in LST and MRT (R-squared value of 0.43 for the LST and 0.35 for the MRT regression model).

Table 3 presents standardized regression coefficients with only GSV-driven variables included in models. As this table suggests, most of the landscape features and urban forms metrics, even in lower data resolution, have a statistically significant effect (P-value<0.05) on changing land surface and mean radiant temperature. Moreover, according to this

Table C2
The correlation between SVF, tree, and building in the whole study area and high-density zone.

	Tree	Building
Whole Study Area (SVF)	−0.73	0.14
High-Density Zone (SVF)	−0.32	−0.27

Table C1
Average values of exposure data and vegetation and urban form metrics in the whole study area and high-density zone.

		AT	LST	MRT	Plant	Grass	Tree	Building	SVF	GVI
Whole Study Area	Ave.	82.30	39.9	49.9	0.02	0.05	0.28	0.03	0.69	40.5
	Std.	1.47	4.07	7.39	0.03	0.05	0.14	0.06	0.25	23.19
High-Density Zone	Ave.	82.38	42.9	52.03	0.01	0.02	0.17	0.10	0.75	21.75
	Std.	1.26	3.18	5.55	0.01	0.03	0.11	0.09	0.20	16.38
Net average change		−0.08	−3.00*	−2.13*	0.01*	0.03*	0.11*	−0.07*	−0.06*	18.75*

* Significant at 95% confidence level.

table, the direction and magnitude of the effect of GSV-driven variables showed a consistent trend among higher and lower resolutions of LST and MRT data. This finding demonstrates the application of GSV-driven variables in explaining land surface and mean radiant temperature variations. Moreover, it suggests the usefulness of the lower resolutions of LST and MRT data for representing spatial heat heterogeneity in the case of high-resolution data paucity.

3.3. Effect magnitude of specific landscape features and urban form metrics on temperatures variations in the whole study area and high-density zones

According to Table 4, plants in both the whole study area and high-density zones are significantly (with P-value<0.05) related to the AT, LST, and MRT. As it was the pattern with the full dataset, vegetation parameters (plants and grass) showed a negative relationship with AT, LST, and MRT. However, the magnitude of their effects on AT, LST, and MRT was slightly different, with high-density zones having a slightly reduced effect of plants and grass on air temperature (SRC value of −0.11 and −0.18 for the whole study area compared to −0.06 and −0.18 for the high-density zones).

The direction and strength of the relationship between buildings and temperature-related data were found to be different in the whole study area and high-density zones. For example, while buildings showed a statistically insignificant positive (+0.01) relationship with MRT for the whole study area, in the high-density zones, buildings had a significant negative effect (−0.12) on MRT. This result implies that the 1% increase in building density would decrease MRT by 0.12 and is related to the shading effect of buildings in high-density residential and commercial zones. However, the relationship between the buildings and LST (both in the whole study area and high-density zones) remained positive, suggesting that an increase in building density would lead to a rise in the land surface temperature. The association of land cover (in this case, built areas) and land surface temperature can explain such a pattern. The relationship between air temperature and buildings both in the whole study area and the high-density zones was found to be statistically insignificant.

Table 4 also shows the significant positive relationship between SVF and all types of temperature data in the whole study area and high-density zones, emphasizing that the increase in the street's openness would lead to a rise in temperatures. SVF showed the most substantial effect on changing MRT. However, the magnitude of this association proved to be smaller for the high-density area compared to the whole study area. This difference was especially significant for the LST data, where the magnitude of association from 0.26 dropped to 0.09.

4. Discussion

4.1. The spatial resolution effect

Downgrading the resolution of both raster-based heat exposure data examined in this study (LST and MRT) didn't affect the R-squared values of regression models significantly. For the LST data, the explanatory power of predictors for explaining the variations in land surface temperature remained almost stable up to the downgraded resolution of 500 ft (~152 m). It's worth noting that, as described in the "Data" section, we used down-sampled Landsat TIR sensor data with a resolution of 30 m (approximately 100 feet). As the native resolution of Landsat TIR sensor data is 100 m, aggregating pixel sizes of our data and reducing the resolution to this range did not significantly reduce the accuracy of the gained information. This may explain why the R-squared values of LST regression models using data with a resolution in the range of about 100 m did not decrease significantly.

For the MRT data, up to the downgraded resolution of 48 ft (~15 m), the R-squared values of the regression models remained within the range of the original data resolution. These findings support the use of lower-

resolution LST and MRT data in explaining temperature variations when higher-resolution data is unavailable due to resource and computational constraints. Dropping the R-squared values of the regression models with the downgraded data resolution can be explained by the Modifiable Areal Unit Problem (MAUP). Coarser units of analysis resulting from aggregating the adjacent pixels and smoothing pixel values introduce spatial data quality concerns (Griffith et al., 2015; Marceau, 1999). Despite this fact, according to studies such as Sobrino et al. (2012), the spatial resolution of LST data could be as low as 165 ft (~50 m) to represent the differences in urban heat island effect between districts (Sobrino et al., 2012). Wu et al. (2019) also found no significant change in the association between adverse health outcomes and land surface temperature at three spatial resolutions (zip codes, 12.5 km grids, and 1 km grids) (Wu et al., 2019). Although these findings align with the current study's results and support lower data use to represent variations in MRT and LST, data resolution should be chosen based on the specific purpose of the studies and careful consideration of the physical phenomenon being represented. This notion is especially crucial when producing heat risk hotspots using spatial vulnerability and exposure data, while the data is usually aggregated to match the employed spatial units (e.g., census tract, postal code) (Ho et al., 2015). Results of this study have important implications for heat-related modeling and studies that use heat exposure data for estimating heat morbidity (Wang et al., 2021) and the citizen's need during extreme heat events (Kianmehr & Pamukcu, 2021).

4.2. The explanatory power of different groups of vulnerability indicators

Examining different groups of vulnerability indicators showed that population and zone-based variables have the most important impacts in explaining the variations in air temperature. The association of air temperature with socio-demographics and land use/ land cover characteristics can explain this observation (Ngarambe et al., 2021). Moreover, in our analyses, landscape features and urban form metrics (GSV-driven variables) showed the highest explanatory power for explaining LST and MRT variations. It is widely acknowledged that land surface temperature is strongly influenced by local landscape features (e.g., plants, trees, and grass) and urban form metrics (e.g., urban geometry, the sky view factor, aspect ratio, etc.) (Gage & Cooper, 2017; Yang et al., 2021). Recent studies have shown the application of GSV images for estimating sky view factor, urban greenery, shade provision, and residents' outdoor heat exposure (Li, 2021b; Li & Ratti, 2018, 2019). In this study, GSV-driven variables, even in the lowest resolution of data, showed moderate explanatory power for explaining the variations in LST and MRT data. However, the lower adjusted R-squared values of regression models with air temperature as the dependent variable in this study can be attributed to the more compound relationship between local air temperature and factors such as anthropogenic activities, physical and landscape characteristics (Amani-Beni et al., 2022).

4.3. The effect magnitude of specific landscape features and urban form metrics

For vegetation parameters examined in this study (plant and grass), the direction of their effects on temperatures was negative and consistent across all three types of exposure data, confirming the results of previous studies (Dimoudi & Nikolopoulou, 2003; Giridharan et al., 2008). The most notable impact of buildings observed on MRT in high-density zones where a significant negative effect was recorded (−0.12), and this pattern was not observed with LST. A similar pattern regarding the shading effect of buildings and their role in reducing MRT levels in urban environments was observed in previous studies (Lindberg & Grimmond, 2011; Nasrollahi et al., 2021). The role of the sky view factor in changing temperature was also significant. The direction of the SVF effect on temperature exposure data was consistent (a significant

positive effect) across all variables in the whole study area and high-density zones. This finding is in line with the other studies. For example, a study in Phoenix, Arizona, showed that the sky view factor derived from GSV images has a statistically significant positive correlation with daytime and nighttime LST (0.52 and 0.11, respectively) (Zhang et al., 2019). Similarly, in a study in Beijing, China, it was shown that highly shaded areas (SVF<0.3) would significantly reduce the frequency of thermal discomfort (He et al., 2015). To this, our study additionally shows that the effect magnitude of this variable decreased in high-density zones. This might be explained by the sparse and homogenized tree density in high-density zones (Table C1). As trees play a central role in controlling SVF, this can affect the strength of the association between SVF and temperatures. However, in high-density areas, buildings show a strong negative relationship with the SVF (Table C2), suggesting the increase in buildings would decrease the street openness (SVF) and would ultimately help with lowering temperatures (especially mean radiant temperature). This finding provides an important piece of evidence about the usefulness of other street-level elements than trees (such as buildings) to impede direct solar radiation and improve thermal comfort in urban environments.

4.4. Limitations and future research

This study has its limitations. In terms of data sources, we only included air temperature, land surface temperature, and mean radiant temperature at a range of resolutions as the heat exposure variables. However, there are also other heat indexes such as Wet Bulb Globe Temperature (WGBT), Universal Thermal Comfort Index (UTCI), Physiological Equivalent Temperature (PET), and Predicted Mean Vote (PMV) that involve human body characteristics and humidity, radiation, and wind speed besides temperature to measure thermal comfort level (Höppe, 1999; Jendritzky et al., 2012; Wei et al., 2022a, 2022b). Investigating the appropriate resolution ranges of such heat measures can be the subject of future research. Moreover, in this study, we just focused on a limited range of spatial resolution, while the effect of temporal resolution of data is also substantial and requires further investigation. Also, a wider range of spatial data resolution can be applied for more comprehensive conclusions. In terms of methods, we just employed one resampling technique (bilinear interpolation) for changing data resolutions. However, different resampling techniques (cubic convolution, nearest neighbor, etc.) might slightly change the results. Therefore, further research is needed to study the choice of resampling method and its influence on the results. Finally, we note the current analysis was conducted only for Atlanta, so the results are not generalizable to locations with different climates, landscapes, and demographic characteristics. Cross-site evaluations can be performed in future research to explore the consistency of observed results.

5. Conclusion

In this paper, we tried to study the satisfactory range of exposure data resolutions for accurately representing spatial temperature variations. Moreover, by including different types of physical and social vulnerability metrics, we explored which groups of vulnerability indicators can better explain the variations in temperature-related data. Further, we investigated the effect of specific landscape features and urban form metrics on changing temperatures in urban environments. Finally, we compared the effect of those variables on temperatures in the whole study area and high-density zones to check for the role of specific street-level elements in providing shading and thermal comfort.

The results of this study revealed that downgrading resolutions of land surface temperature (up to 152 m) and mean radiant temperature data (up to 15 m) would not substantially reduce the power of social and physical vulnerability metrics in explaining the variations in temperatures. Therefore, the lower resolution of LST and MRT data may still satisfactorily represent spatial urban temperature variations. Moreover,

among vulnerability indicators studied in this paper, landscape features and urban form metrics showed the highest explanatory power in regression models. While the sky view factor proved to have the most influence in changing temperatures in the whole study area, buildings showed a significant effect on reducing the mean radiant temperature (with the SRC value of −0.12) in high-density zones. These findings highlight the usefulness of street-level elements in providing shading and thermal comfort in high-density urban areas. The results of this study provide insights vis-a-vis appropriate sets of data and relevant resolution of temperature measurements for representing spatial urban heat variations which have important implications for heat-related policies and planning.

Declaration of Competing Interest

None.

Data availability

Data will be made available on request.

Appendix A. Spatial autocorrelation effect

We used Moran's I test to check for the spatial autocorrelation effect (the correlation among observation points due to the spatial proximity). The positive values of Moran's I test for AT, LST, and MRT and the (P-value<0.001) verified the spatial autocorrelation hypothesis in our data (Table A1). To address the concerns about the validity of OLS regression results due to the presence of spatial autocorrelation effect, we followed two common approaches. First, to minimize the potential effect of spatial autocorrelation, we randomly selected 3000 points (about one-third of the total observation points) to include in our OLS regression analyses. Second, using GeoDa software, an exploratory spatial data analysis tool, we ran two common spatial regression models called spatial lag model (SLM) and spatial error model (SEM) to compare the results with the OLS method. According to our analyses, the R-squared values of the OLS model appeared to be less than the SLM and SEM models (Table A2), suggesting the absence of bias due to the autocorrelation effect in the OLS method. Moreover, no significant difference in the value and direction of regression coefficients of SLM, SEM, and OLS methods was noticed. So, based on these observations, we proceeded with the OLS model with the random selection of observation points. We shall note here that this choice was also made based on the capability of the OLS method to include zone-based categorical variables in regression analyses which were important for the purpose of this study.

Table A1 represents the Moran's I test using the total observation points to detect the potential spatial autocorrelation effect

Table A2 represents the R-squared values of SLM, SEM, and OLS method using sampled observation points; AT, LST, and MRT as dependent variables; and street-level and population-based variables as

independent variables (Table 2).

Appendix B. F-tests results of nested models

(Table B1, Table B2).

Appendix C. Comparison of the whole study area and high-density zone

(Appendix C)(Table C1, Table C2).

References

Abson, D. J., Dougill, A. J., & Stringer, L. C. (2012). Using principal component analysis for information-rich socio-ecological vulnerability mapping in Southern Africa. *Applied Geography, 35*, 515–524. https://doi.org/10.1016/j.apgeog.2012.08.004

Adger, W. N. (2006). Vulnerability. *Global Environmental Change, 16*, 268–281. https://doi.org/10.1016/j.gloenvcha.2006.02.006. Resilience, Vulnerability, and Adaptation: A Cross-Cutting Theme of the International Human Dimensions Programme on Global Environmental Change.

Amani-Beni, M., Chen, Y., Vasileva, M., Zhang, B., & Xie, G. (2022). Quantitative-spatial relationships between air and surface temperature, a proxy for microclimate studies in fine-scale intra-urban areas? *Sustainable Cities and Society, 77*, Article 103584. https://doi.org/10.1016/j.scs.2021.103584

Berardi, U., Jandaghian, Z., & Graham, J. (2020). Effects of greenery enhancements for the resilience to heat waves: A comparison of analysis performed through mesoscale (WRF) and microscale (Envi-met) modeling. *The Science of the Total Environment, 747*, Article 141300. https://doi.org/10.1016/j.scitotenv.2020.141300

Chakraborty, T., Hsu, A., Manya, D., & Sheriff, G. (2019). Disproportionately higher exposure to urban heat in lower-income neighborhoods: A multi-city perspective. *Environmental Research Letters, 14*, Article 105003. https://doi.org/10.1088/1748-9326/ab3b99

Chen, T. L. (2021). Mapping temporal and spatial changes in land use and land surface temperature based on MODIS data. *Environmental Research, 196*, Article 110424. https://doi.org/10.1016/j.envres.2020.110424

Chen, Y., Shan, B., & Yu, X. (2022). Study on the spatial heterogeneity of urban heat islands and influencing factors. *Building and Environment, 208*, Article 108604. https://doi.org/10.1016/j.buildenv.2021.108604

Chen, Y., Shu, B., Zhang, R., & Amani-Beni, M. (2023). LST determination of different urban growth patterns: A modeling procedure to identify the dominant spatial metrics. *Sustainable Cities and Society, 92*, Article 104459. https://doi.org/10.1016/j.scs.2023.104459

Conlon, K. C., Mallen, E., Gronlund, C. J., Berrocal, V. J., Larsen, L., & O, 'NMS. (2020). Mapping human vulnerability to extreme heat: A critical assessment of heat vulnerability indices created using principal components analysis. *Environmental Health Perspectives, 128*, Article 097001. https://doi.org/10.1289/EHP4030

Cutter, S. L., Boruff, B. J., & Shirley, W. L. (2003). Social vulnerability to environmental hazards *: Social vulnerability to environmental hazards. *Social Science Quarterly, 84*, 242–261. https://doi.org/10.1111/1540-6237.8402002

Cutter, S. L., & Finch, C. (2008). Temporal and spatial changes in social vulnerability to natural hazards. *Proceedings of the National Academy of Sciences, 105*, 2301–2306. https://doi.org/10.1073/pnas.0710375105

Deilami, K., Kamruzzaman, M., & Hayes, J. F. (2016). Correlation or causality between land cover patterns and the urban heat island effect? Evidence from Brisbane, Australia. *Remote Sensing, 8*, 716. https://doi.org/10.3390/rs8090716

Deilami, K., Kamruzzaman, Md., & Liu, Y. (2018). Urban heat island effect: A systematic review of spatio-temporal factors, data, methods, and mitigation measures. *International Journal of Applied Earth Observation and Geoinformation, 67*, 30–42. https://doi.org/10.1016/j.jag.2017.12.009

Dialesandro, J., Brazil, N., Wheeler, S., & Abunnasr, Y. (2021). Dimensions of thermal inequity: Neighborhood social demographics and urban heat in the Southwestern U.S. *International Journal of Environmental Research and Public Health, 18*, 941. https://doi.org/10.3390/ijerph18030941

Dimoudi, A., & Nikolopoulou, M. (2003). Vegetation in the urban environment: Microclimatic analysis and benefits. *Energy and Buildings, 35*, 69–76. https://doi.org/10.1016/S0378-7788(02)00081-6. Special issue on urban research.

Fotheringham, A. S., & Wong, D. W. S. (1991). The modifiable areal unit problem in multivariate statistical analysis. *Environment and Planning A: Economy and Space, 23*, 1025–1044. https://doi.org/10.1068/a231025

Gage, E. A., & Cooper, D. J. (2017). Relationships between landscape pattern metrics, vertical structure and surface urban Heat Island formation in a Colorado suburb. *Urban Ecosystems, 20*, 1229–1238. https://doi.org/10.1007/s11252-017-0675-0

Giridharan, R., Lau, S. S. Y., Ganesan, S., & Givoni, B. (2008). Lowering the outdoor temperature in high-rise high-density residential developments of coastal Hong Kong: The vegetation influence. *Building and Environment, 43*, 1583–1595. https://doi.org/10.1016/j.buildenv.2007.10.003

Griffith, D. A., Wong, D. W., & Chun, Y. (2015). Uncertainty-related research issues in spatial analysis. *Uncertainty modelling and quality control for spatial data*. CRC Press.

Guha, S., Govil, H., Dey, A., & Gill, N. (2018). Analytical study of land surface temperature with NDVI and NDBI using Landsat 8 OLI and TIRS data in Florence and Naples city, Italy. *European Journal of Remote Sensing, 51*, 667–678. https://doi.org/10.1080/22797254.2018.1474494

Guillard-Gonçalves, C., & Zêzere, J. L. (2018). Combining social vulnerability and physical vulnerability to analyse landslide risk at the municipal scale. *Geosciences, 8*, 294. https://doi.org/10.3390/geosciences8080294

Gunawardena, K., & Steemers, K. (2019). Adaptive comfort assessments in urban neighbourhoods: Simulations of a residential case study from London. *Energy and Buildings, 202*, Article 109322. https://doi.org/10.1016/j.enbuild.2019.07.039

Habeeb, D., Vargo, J., & Stone, B. (2015). Rising heat wave trends in large US cities. *Natural Hazards, 76*, 1651–1665. https://doi.org/10.1007/s11069-014-1563-z

Habitat. (2017). *The new urban agenda [WWW document]*. Habitat III. URL https://habitat3.org/the-new-urban-agenda/ accessed 7.29.22.

Harlan, S. L., Brazel, A. J., Prashad, L., Stefanov, W. L., & Larsen, L. (2006). Neighborhood microclimates and vulnerability to heat stress. *Social Science and Medicine, 63*, 2847–2863. https://doi.org/10.1016/j.socscimed.2006.07.030

Hart, M. A., & Sailor, D. J. (2009). Quantifying the influence of land-use and surface characteristics on spatial variability in the urban heat island. *Theoretical and Applied Climatology, 95*, 397–406. https://doi.org/10.1007/s00704-008-0017-5

He, X., Miao, S., Shen, S., Li, J., Zhang, B., Zhang, Z., et al. (2015). Influence of sky view factor on outdoor thermal environment and physiological equivalent temperature. *International Journal of Biometeorology, 59*, 285–297. https://doi.org/10.1007/s00484-014-0841-5

Ho, H. C., Knudby, A., & Huang, W. (2015). A spatial framework to map heat health risks at multiple scales. *International Journal of Environmental Research and Public Health, 12*, 16110–16123. https://doi.org/10.3390/ijerph121215046

Hoffman, J. S., Shandas, V., & Pendleton, N. (2020). The effects of historical housing policies on resident exposure to intra-urban heat: A study of 108 US urban areas. *Climate, 8*, 12. https://doi.org/10.3390/cli8010012

Höppe, P. (1999). The physiological equivalent temperature – a universal index for the biometeorological assessment of the thermal environment. *International Journal of Biometeorology, 43*, 71–75. https://doi.org/10.1007/s004840050118

Hsu, A., Sheriff, G., Chakraborty, T., & Manya, D. (2021). Disproportionate exposure to urban heat island intensity across major US cities. *Nature Communications, 12*, 2721. https://doi.org/10.1038/s41467-021-22799-5

Jelinski, D. E., & Wu, J. (1996). The modifiable areal unit problem and implications for landscape ecology. *Landscape Ecology, 11*, 129–140. https://doi.org/10.1007/BF02447512

Jendritzky, G., de Dear, R., & Havenith, G. (2012). UTCI—Why another thermal index? *International Journal of Biometeorology, 56*, 421–428. https://doi.org/10.1007/s00484-011-0513-7

Johnson, D. P., Stanforth, A., Lulla, V., & Luber, G. (2012). Developing an applied extreme heat vulnerability index utilizing socioeconomic and environmental data. *Applied Geography, 35*, 23–31. https://doi.org/10.1016/j.apgeog.2012.04.006

Ju, H., Niu, C., Zhang, S., Jiang, W., Zhang, Z., Zhang, X., … Cui, Y. (2021). Spatiotemporal patterns and modifiable areal unit problems of the landscape ecological risk in coastal areas: A case study of the Shandong Peninsula, China. *Journal of Cleaner Production, 310*, Article 127522. https://doi.org/10.1016/j.jclepro.2021.127522

Karanja, J., & Kiage, L. (2021). Perspectives on spatial representation of urban heat vulnerability. *The Science of the Total Environment, 774*, Article 145634. https://doi.org/10.1016/j.scitotenv.2021.145634

Keith, L., & Meerow, S. (2022). *Planning for urban heat resilience*. American Planning Association.

Kianmehr, A., & Lim, T. C. (2022). Quantifying interactive cooling effects of morphological parameters and vegetation-related landscape features during an extreme heat event. *Climate, 10*, 60. https://doi.org/10.3390/cli10040060

Kianmehr, A., & Pamukcu, D.. *Analyzing citizens' needs during an extreme heat event, based on 311 service requests: A case study of the 2021 heatwave in Vancouver, British*. https://par.nsf.gov/biblio/10354938-analyzing-citizens-needs-during-extreme-heat-event-based-service-requests-case-study-heatwave-vancouver-british-columbia.

Larsen, L., Gronlund, C. J., Ketenci, K. C., Harlan, S. L., Hondula, D. M., Stone, B., … O'Neill, M. S. (2022). Safe at home? *Journal of the American Planning Association*, 1–13. https://doi.org/10.1080/01944363.2022.2087724

Li, X. (2021a). Investigating the spatial distribution of resident's outdoor heat exposure across neighborhoods of Philadelphia, Pennsylvania using urban microclimate modeling. *Sustainable Cities and Society, 72*, Article 103066. https://doi.org/10.1016/j.scs.2021.103066

Li, X. (2021b). Examining the spatial distribution and temporal change of the green view index in New York City using Google Street View images and deep learning. *Environment and Planning B: Urban Analytics and City Science, 48*, 2039–2054. https://doi.org/10.1177/2399808320962511

Li, X., & Ratti, C. (2018). Mapping the spatial distribution of shade provision of street trees in Boston using Google Street View panoramas. *Urban Forestry and Urban Greening, 31*, 109–119. https://doi.org/10.1016/j.ufug.2018.02.013

Li, X., & Ratti, C. (2019). Mapping the spatio-temporal distribution of solar radiation within street canyons of Boston using Google Street View panoramas and building height model. *Landscape and Urban Planning, 191*, Article 103387. https://doi.org/10.1016/j.landurbplan.2018.07.011

Li, X., Zhang, C., Li, W., Kuzovkina, Y. A., & Weiner, D. (2015a). Who lives in greener neighborhoods? The distribution of street greenery and its association with residents' socioeconomic conditions in Hartford, Connecticut, USA. *Urban Forestry and Urban Greening, 14*, 751–759. https://doi.org/10.1016/j.ufug.2015.07.006

Li, X., Zhang, C., Li, W., Ricard, R., Meng, Q., & Zhang, W. (2015b). Assessing street-level urban greenery using Google Street View and a modified green view index. *Urban Forestry and Urban Greening, 14*, 675–685. https://doi.org/10.1016/j.ufug.2015.06.006

Lindberg, F., & Grimmond, C. S. B. (2011). Nature of vegetation and building morphology characteristics across a city: Influence on shadow patterns and mean

radiant temperatures in London. *Urban Ecosystems, 14*, 617–634. https://doi.org/10.1007/s11252-011-0184-5

Lindberg, F., Holmer, B., & Thorsson, S. (2008). SOLWEIG 1.0 – Modelling spatial variations of 3D radiant fluxes and mean radiant temperature in complex urban settings. *International Journal of Biometeorology, 52*, 697–713. https://doi.org/10.1007/s00484-008-0162-7

Marceau, D. J. (1999). The scale issue in the social and natural sciences. *Canadian Journal of Remote Sensing, 25*, 347–356. https://doi.org/10.1080/07038992.1999.10874734

Meng, Q., Zhang, L., Sun, Z., Meng, F., Wang, L., & Sun, Y. (2018). Characterizing spatial and temporal trends of surface urban heat island effect in an urban main built-up area: A 12-year case study in Beijing, China. *Remote Sensing of Environment, 204*, 826–837. https://doi.org/10.1016/j.rse.2017.09.019

Middel, A., Lukasczyk, J., Zakrzewski, S., Arnold, M., & Maciejewski, R. (2019). Urban form and composition of street canyons: A human-centric big data and deep learning approach. *Landscape and Urban Planning, 183*, 122–132. https://doi.org/10.1016/j.landurbplan.2018.12.001

Mukherjee, F., & Singh, D. (2020). Assessing land use–land cover change and its impact on land surface temperature using LANDSAT data: A comparison of two urban areas in India. *Earth Systems and Environment, 4*, 385–407. https://doi.org/10.1007/s41748-020-00155-9

Mushore, T. D., Mutanga, O., Odindi, J., & Dube, T. (2018). Determining extreme heat vulnerability of Harare Metropolitan City using multispectral remote sensing and socio-economic data. *Journal of Spatial Science, 63*, 173–191. https://doi.org/10.1080/14498596.2017.1290558

Nasrollahi, N., Namazi, Y., & Taleghani, M. (2021). The effect of urban shading and canyon geometry on outdoor thermal comfort in hot climates: A case study of Ahvaz, Iran. *Sustainable Cities and Society, 65*, Article 102638. https://doi.org/10.1016/j.scs.2020.102638

Ngarambe, J., Oh, J. W., Su, M. A., Santamouris, M., & Yun, G. Y. (2021). Influences of wind speed, sky conditions, land use and land cover characteristics on the magnitude of the urban heat island in Seoul: An exploratory analysis. *Sustainable Cities and Society, 71*, Article 102953. https://doi.org/10.1016/j.scs.2021.102953

Oke, T. R. (1987). *Boundary layer climates*. Psychology Press.

Openshaw, S. (1984). *The modifiable areal unit problem*. Concepts Tech. Mod. Geogr.

Peng, J., Hu, Y., Dong, J., Liu, Q., & Liu, Y. (2020). Quantifying spatial morphology and connectivity of urban heat islands in a megacity: A radius approach. *The Science of the Total Environment, 714*, Article 136792. https://doi.org/10.1016/j.scitotenv.2020.136792

Preston, B. L., Yuen, E. J., & Westaway, R. M. (2011). Putting vulnerability to climate change on the map: A review of approaches, benefits, and risks. *Sustainability Science, 6*, 177–202. https://doi.org/10.1007/s11625-011-0129-1

Schwarz, N., Lautenbach, S., & Seppelt, R. (2011). Exploring indicators for quantifying surface urban heat islands of European cities with MODIS land surface temperatures. *Remote Sensing of Environment, 115*, 3175–3186. https://doi.org/10.1016/j.rse.2011.07.003

Sobrino, J. A., Oltra-Carrió, R., Sòria, G., Bianchi, R., & Paganini, M. (2012). Impact of spatial resolution and satellite overpass time on evaluation of the surface urban heat island effects. Remote Sens. Environ *Remote Sensing of Urban Environments, 117*, 50–56. https://doi.org/10.1016/j.rse.2011.04.042.

Song, J., Huang, B., Kim, J. S., Wen, J., & Li, R. (2020). Fine-scale mapping of an evidence-based heat health risk index for high-density cities: Hong Kong as a case study. *The Science of the Total Environment, 718*, Article 137226. https://doi.org/10.1016/j.scitotenv.2020.137226

Sun, X., Crittenden, J. C., Li, F., Lu, Z., & Dou, X. (2018). Urban expansion simulation and the spatio-temporal changes of ecosystem services, a case study in Atlanta Metropolitan area, USA. *Science of the Total Environment, 622–623*, 974–987. https://doi.org/10.1016/j.scitotenv.2017.12.062

Turner, B. L., Kasperson, R. E., Matson, P. A., McCarthy, J. J., Corell, R. W., Christensen, L., et al. (2003). A framework for vulnerability analysis in sustainability science. *Proceedings of the National Academy of Sciences, 100*, 8074–8079. https://doi.org/10.1073/pnas.1231335100

Uejio, C. K., Wilhelmi, O. V., Golden, J. S., Mills, D. M., Gulino, S. P., & Samenow, J. P. (2011). Intra-urban societal vulnerability to extreme heat: The role of heat exposure and the built environment, socioeconomics, and neighborhood stability. *Health Place, Geographies of Care, 17*, 498–507. https://doi.org/10.1016/j.healthplace.2010.12.005

Mapping campaigns. (2022). URL https://www.heat.gov/pages/mapping-campaigns (accessed 9.10.22).

United States Census Bureau, U.C., (2021). Metropolitan and micropolitan. Census.gov. URL https://www.census.gov/programs-surveys/metro-micro.html (accessed 8.9.22).

USGS, (2023). Landsat 9 | U.S. geological survey. URL https://www.usgs.gov/landsat-missions/landsat-9 (accessed 3.29.23).

Voelkel, J., Hellman, D., Sakuma, R., & Shandas, V. (2018). Assessing vulnerability to urban heat: A study of disproportionate heat exposure and access to refuge by socio-demographic status in Portland, Oregon. *International Journal of Environmental Research and Public Health, 15*, 640. https://doi.org/10.3390/ijerph15040640

Wang, C., Solís, P., Villa, L., Khare, N., Wentz, E. A., & Gettel, A. (2021). Spatial modeling and analysis of heat-related morbidity in Maricopa County, Arizona. *Journal of Urban Health, 98*, 344–361. https://doi.org/10.1007/s11524-021-00520-7

Wei, D., Yang, L., Bao, Z., Lu, Y., & Yang, H. (2022a). Variations in outdoor thermal comfort in an urban park in the hot-summer and cold-winter region of China. *Sustainable Cities and Society, 77*, Article 103535. https://doi.org/10.1016/j.scs.2021.103535

Wei, D., Zhao, G., Liu, S., & Yang, L. (2022b). Indoor thermal comfort in a rural dwelling in southwest China. *Frontiers in Public Health, 10*, Article 1029390. https://doi.org/10.3389/fpubh.2022.1029390

Weng, Q., Liu, H., & Lu, D. (2007). Assessing the effects of land use and land cover patterns on thermal conditions using landscape metrics in city of Indianapolis, United States. *Urban Ecosystem, 10*, 203–219. https://doi.org/10.1007/s11252-007-0020-0

Wilson, B. (2020). Urban Heat Management and the Legacy of Redlining. *Journal of the American Planning Association, 86*, 443–457. https://doi.org/10.1080/01944363.2020.1759127

Wu, C. Y. H., Zaitchik, B. F., Swarup, S., & Gohlke, J. M. (2019). Influence of the spatial resolution of the exposure estimate in determining the association between heat waves and adverse health outcomes. *Annals of the American Association of Geographers, 109*, 875–886. https://doi.org/10.1080/24694452.2018.1511411

Xu, T., Sathaye, J., Akbari, H., Garg, V., & Tetali, S. (2012). Quantifying the direct benefits of cool roofs in an urban setting: Reduced cooling energy use and lowered greenhouse gas emissions. *Building and Environment, 48*, 1–6. https://doi.org/10.1016/j.buildenv.2011.08.011

Yang, C., Zhu, W., Sun, J., Xu, X., Wang, R., Lu, Y., et al. (2021). Assessing the effects of 2D/3D urban morphology on the 3D urban thermal environment by using multi-source remote sensing data and UAV measurements: A case study of the snow-climate city of Changchun, China. *Journal of Cleaner Production, 321*, Article 128956. https://doi.org/10.1016/j.jclepro.2021.128956

Yang, Q., Huang, X., & Li, J. (2017). Assessing the relationship between surface urban heat islands and landscape patterns across climatic zones in China. *Scientific Reports, 7*, 9337. https://doi.org/10.1038/s41598-017-09628-w

Zhang, Y., Middel, A., & Turner, B. L. (2019). Evaluating the effect of 3D urban form on neighborhood land surface temperature using Google Street View and geographically weighted regression. *Landscape Ecology, 34*, 681–697. https://doi.org/10.1007/s10980-019-00794-y

Zhao, H., Shi, J., Qi, X., Wang, X., & Jia, J.. Pyramid scene parsing network. Recognition. https://openaccess.thecvf.com/content_cvpr_2017/html/Zhao_Pyramid_Scene_Parsing_CVPR_2017_paper.html.

Zhou, W., Qian, Y., Li, X., Li, W., & Han, L. (2014). Relationships between land cover and the surface urban heat island: Seasonal variability and effects of spatial and thematic resolution of land cover data on predicting land surface temperatures. *Landscape Ecology, 29*, 153–167. https://doi.org/10.1007/s10980-013-9950-5